Novel Full-Cycle-Coupler-Based Optical Add–Drop Multiplexer and Performance Characteristics at 40-Gb/s WDM Networks

Christos Riziotis, *Member, IEEE, Member, OSA*, and Mikhail N. Zervas, *Member, IEEE*

***Abstract*—A novel configuration of an interferometric device, based on a full-cycle full (100%) coupler structure, loaded with a Bragg grating symmetrically placed into the uniform coupler waist, is proposed for use as an optical add–drop multiplexer (OADM) with simultaneously optimized add and drop actions. A general method for designing a suitable Bragg grating for optimal inscription in to the uniform coupler waist is also proposed for use in to the device design and development. The performance of the device is characterized at 40-Gb/s wavelength-division-multiplexing (WDM) networks using theoretical systems simulations and is compared directly with other alternative OADM architectures.**

***Index Terms*—Couplers, gratings, modeling, optical communication, optical components, optical waveguide filters, simulation, switches, wavelength-division multiplexing (WDM).**

I. Introduction

OPTICAL add–drop multiplexers (OADMs) are key components for wavelength-division multiplexing (WDM) in optical communication systems. Basic four-port devices that add and/or drop a particular WDM channel are going to be of great importance in future optical networks. OADMs can be used as simple components, which serve a single subscriber in a node of an optical network, or as building blocks of more complicated modules as optical cross-connects and switch matrices. Simple OADM configurations, using the unique spectral characteristics of phase Bragg gratings, appear to be very promising solutions intended to find applications in high-performance WDM systems.

A number of different Bragg-grating-based four-port OADM configurations have been proposed and implemented to date. They are generally divided in two main categories, the noninterferometric and interferometric configurations.

A widely employed noninterferometric OADM is the well-known configuration with the two optical circulators (OCs) [1]. This simple OADM makes direct use of the reflection properties of a Bragg grating, written in a single-mode fiber and is frequently used as a benchmark in the sense that it provides excellent crosstalk performance and negligible back reflections. However, it suffers from relatively high insertion loss ($\sim$1 dB), it is bulky and expensive, and it cannot be easily integrated. More compact noninterferometric OADMs, without the use of circulators, have been demonstrated in fiber or channel waveguide implementations [2], [3]. A comparison of the main representatives of this category can be found in [4] and [5].

In the category of interferometric OADMs now, the most representative device is the one based in the Mach–Zehnder interferometer (MZI) [6]–[10]. Perfectly matched MZI-based OADMs, with identical Bragg gratings in each arm, can potentially result in an ideal performance, better than the one of OC-based OADMs, since they exhibit no backreflections and need no extra components, i.e. circulators or isolators. Additionally they can provide very low insertion losses ($\sim$0.1 dB) and they can be fully integrated. However, grating mismatches and interferometer-arm imperfections compromise severely the OADM performance, resulting in strong backreflections and spectral distortions. In this case, careful post-processing and trimming is required [10]. In addition, two extra isolators are quite likely to be required at the two input ports to avoid the deleterious effects of backreflections, making the total extra-component count equal to the OC-based devices.

Interferometric OADMs based on full coupler (FC)-based configurations have been proposed as an alternative design to MZI configurations. In the MZI configuration, any imbalance of the order of one wavelength of light can degrade drastically the performance of the device because the interference takes place between different waveguides. In the FC configuration, the allowable imbalance for the same degradation is much greater—of the order of the coupling length—because the interference now is based on the beating between the normal modes of the waist waveguide.

To date, the majority of the demonstrated coupler-based OADMs are based on a half-cycle coupler (HCC) configuration with a Bragg grating written into the uniform coupler waist [11]. This device cannot give fully optimized add and drop actions simultaneously due to the required asymmetric inscription of the grating with respect to the centre of the coupler waist [12] in order to achieve an optimized, spectrally flat amplitude response at the drop port. In this case, the add action can be severely compromised [13], [14], especially in high-bit-rate (10, 40 Gb/s) applications.

This paper proposes and describes a novel OADM based on a full-cycle full (100%) coupler (FCC) configuration where

Manuscript received August 15, 2002; revised April 28, 2003. This work was supported by Pirelli CAVI S.p.A., Milan, Italy.

C. Riziotis was with the Optoelectronics Research Centre, University of Southampton, Southampton SO17 1BJ, U.K. He is now with the Optical Communications Laboratory, Department of Informatics and Telecommunications, University of Athens, Panepistimiopolis, Ilyssia, GR-15784 Athens, Greece (e-mail: Christos.Riziotis@ieee.org).

M. N. Zervas is with the Optoelectronics Research Centre, University of Southampton, Southampton SO17 1BJ, U.K., and also with Southampton Photonics, Inc., Southampton SO16 7NS, U.K.

Digital Object Identifier 10.1109/JLT.2003.815501

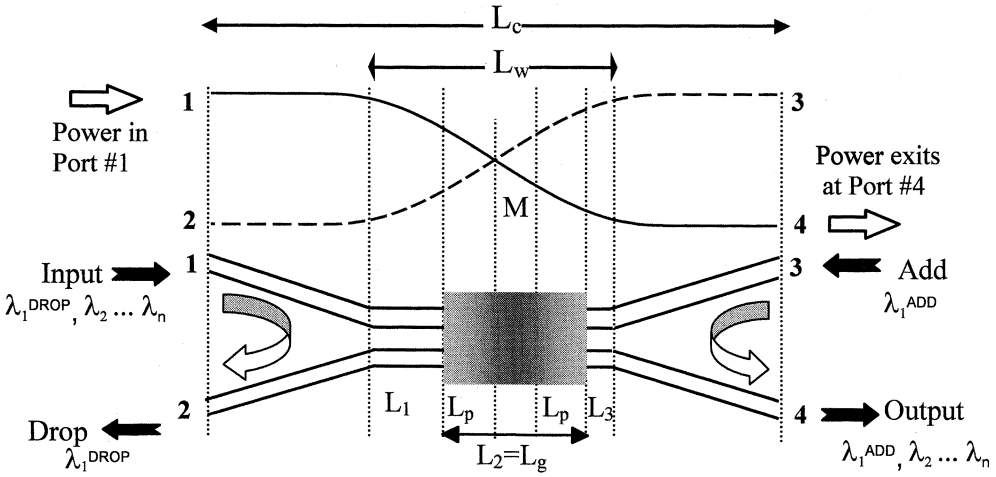

Fig. 1. Schematic of the half-cycle coupler (HCC) OADM with the power evolution along the full coupler. The OADM is configured in an asymmetric configuration for optimized drop action.

the optimum placement of the grating in the uniform waist is symmetric with respect to the two ends of the device, thus resulting in fully optimized add and drop actions. The performance of the proposed OADM is theoretically characterized at WDM networks using system simulations in an intensity modulation/direct-detection (IM/DD) system employing nonreturn-to-zero (NRZ) modulation format at 40 Gb/s and is then compared directly to other OADMs.

II. Prior Art of FC-Based OADM: The HCC OADM

The HCC OADM that has been extensively studied [11]–[15] is shown schematically in Fig. 1, together with the power evolution along the coupler. The total length of the coupler is $L_c = Z_c/2$ where Z_c is the beat length between the even and odd supermodes of the coupler. If $\mathrm{n_e}$ and n_o are the effective refractive indexes of the even and odd supermodes, respectively, then the beat length is defined as $Z_c = \lambda/(n_e - n_o)$, where λ is the operating wavelength. Fig. 1 illustrates that a stream of WDM channels enters through Port 1 and the channel at wavelength ${\lambda_1}^{\mathrm{DROP}}$ is reflected by the grating and dropped at Port 2. The grating is placed asymmetrically with respect to the centre of the waist so that its effective reflecting point at the wavelength of interest ${\lambda_1}^{\mathrm{DROP}}$ coincides with the middle point (M) of the coupler. At this point the two supermodes of the coupler are reflected and their destructive interference at Port 1 guarantees that all the power at the wavelength of interest will appear at the drop Port 2. It should be stressed out that the two eigenmodes have different propagation constants and their corresponding reflection spectra are spectrally displaced with respect to each other and, therefore partially overlapping. The bandwidth of the drop response is determined by this overlap.

The analysis and modeling of interferometric devices can be easily performed by decomposing the propagating fields into the even and odd supermodes of the coupler and by calculating the interference between them. However, as in our previous work on modeling of HCC OADMs [14], we have used for the simulation and modeling of the OADM the rigorous and accurate method of normal mode theory, which is presented in detail in [4]. However, the case here is much simpler because symmetry considerations guarantee that these orthogonal normal modes do not cross-couple energy by scattering from the Bragg grating (assuming always that the grating is written perpendicular and placed symmetrically with respect to the waist axis of the coupler). As is illustrated in Fig. 1, in order to configure optimally the OADM, the Bragg grating has to be placed accordingly by taking into account its penetration depth—at the central wavelength of the dropped channel.

Next, we briefly introduce the basic concepts of the time delay and equivalent penetration depth of the reflected light. If $\theta = phase(r)$ is the phase of the reflection coefficient r of the grating, then the time delay for reflected light is

$$\tau = \frac{d\theta}{d\omega} = \frac{d\theta}{dk} \cdot \frac{1}{c_o} \tag{1}$$

where $k = (\omega/c_o) = (2\pi/\lambda)$ and c_o is the speed of light in vacuum. The equivalent penetration depth of a particular wavelength can be estimated by considering the length, which corresponds to half the time delay. Thus

$$L_p = \frac{1}{2} c \cdot \tau = \frac{1}{2} \cdot \frac{c_o}{n} \cdot \frac{d\theta}{dk} \cdot \frac{1}{c_o} = \frac{1}{2 \cdot n} \cdot \frac{d\theta}{dk} \tag{2}$$

where c is the speed of light in the waveguide-grating and n is the average refractive index of the waveguide.

We consider now a typical example of coupler structure and calculate the full response of the OADM. The length of the coupler is $L_c \approx 20$ mm, and the uniform coupler waist length is $L_{\mathrm{w}} = L_1 + L_2 + L_3 \approx 9.6$ mm. The deployed Bragg grating has a sine apodization profile, a length of 4.5 mm, and refractive index modulation 10^{-3} (p-p). The grating exhibits absolute reflectivity of $\sim$45 dB and -3-dB bandwidth of $\sim$1 nm. The penetration depth at the central operating wavelength of 1.55 μm is calculated to be 762 μm.

Fig. 2 shows the reflection spectra of the OADM, which is configured for optimized drop action. At the same graph are shown also the reflectivity spectra of the even and odd modes

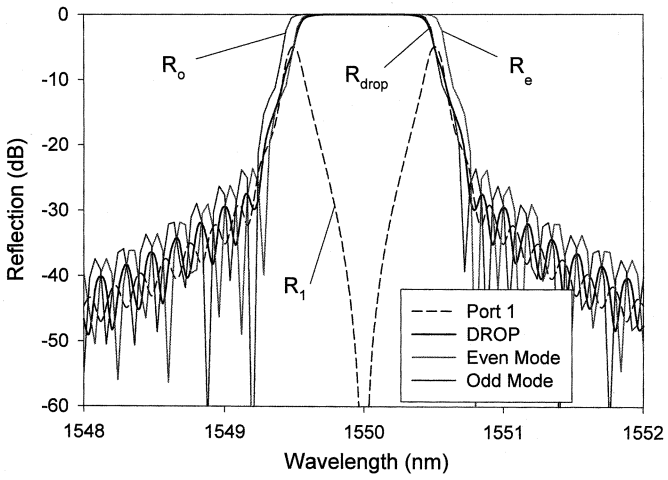

Fig. 2. Spectral response of the HCC-based OADM. The drop action is formed by the partial overlap of the even and odd modes reflection spectra.

R_e and R_o centered, respectively, at wavelengths λ_e, λ_o. The relative spectral displacement is

$$\Delta\lambda = |\lambda_e - \lambda_o| = 2 \cdot (n_e - n_o) \cdot \Lambda_o = \frac{2 \cdot \lambda \cdot \Lambda_o}{Z_c} \quad (3)$$

where Λ_o is the period of the grating.

For optimized drop action, the grating is arranged so that its effective reflection point around the Bragg wavelength coincides with M and therefore drops efficiently around this wavelength. It is obvious that when the device is optimized for channel dropping at Port 2, the channel adding at Port 3 is severely degraded. For simultaneous add-and-drop function, the device can be configured in a symmetrical manner by placing the Bragg grating at the center of the coupler waist $(L_1 = L_3)$. This way, the device will exhibit identical but compromised add and drop actions.

Despite the fact that the grating response is symmetric, the coupler-based OADM response is different under the add and drop actions, depending on the relative grating position. In the first configuration (shown in Fig. 1), the drop action is optimized (O)—by placing the grating inside the waist region asymmetrically with respect to the midpoint M so that $L_1 + L_p = L_{\text{waist}}/2$. In this case, the add action is quite degraded (D) due the fact that the effective reflection point on this grating side is well off the waist midpoint M. If the grating is inscripted symmetrically around the waist midpoint M, then both the effective reflection points are on either side of M and, consequently, the device exhibits identical but compromised (C) add–drop operations [14].

We have shown that deployment of HCC OADMs in a WDM transmission system or in a network topology will lead to a system's performance degradation, especially when filter cascades and filter-laser misalignments are considered [13], [14]. The concatenation of filters with even slightly degraded add–drop spectral characteristics can lead to signal distortion and excessive eye-opening penalty (EOP), when the filters' bandwidth utilization by the transmitting signals' spectrum is very high.

In addition to signal distortion and excessive EOP, the nonoptimized spectral response of the HCC OADM leads to signal attenuation [14]. It should be stressed that, when HCC OADMs are deployed in a network, the resulted system excess loss depends on the configuration of the particular devices and their relative ports' orientation. Thus, the overall loss cannot be easily predicted because it can be dynamically changed and consequently cannot be effectively compensated.

III. Novel Full-Cycle Coupler OADM: The FCC OADM

We propose and describe here a *novel* configuration of an OADM based on a Bragg grating assisted *full-cycle* full coupler, shown schematically in Fig. 3. The Bragg grating is inscripted into the center of the coupler waist, making this way the OADM operation completely symmetric. Deployment of a suitable Bragg grating which matches exactly the geometrical characteristics of the coupler waist allows the optimal implementation of both the add and drop actions with flat-top amplitude spectral characteristics.

The graph in Fig. 3 illustrates the operational principle of the device where a stream of WDM channels enters through Port 1 and the channel at wavelength λ_1^{DROP} is reflected by the grating and *dropped* optimally at Port 2. Reciprocally, the channel λ_1^{ADD} is inserted through Port 4 and is *added* optimally through Port 3, to the stream of the rest of the transmitted WDM channels.

In this novel configuration, the coupler length is equal to the even–odd mode beat length Z_c at the operating wavelength. Theoretically, the OADM could be configured for optimized operation by using two reflectors at points M_1 and M_2 that could reflect the add/drop wavelength. These reflectors could theoretically correspond to the two end points of an ideal very strong grating that extend between these points and exhibit zero penetration depth at the wavelength of interest. In the real case where a Bragg grating is deployed is clear that this should be placed symmetrically in the coupler and should have a suitable length in order to make the penetration points of the light—as coming from the left and right side of the device—coincident with points M_1 and M_2, respectively.

This paper also proproses a general method for the successful design of a Bragg grating with the optimum length and refractive index modulation, for a given reflectivity and apodization profile, in order to be exactly matched to the geometrical characteristics of a given FCC structure.

IV. Design of the FCC-Based OADM

In this section, design rules are proposed for the effective optimized design of the FCC-based OADM. The derivation is based on the geometrical characteristics of the arrangement of the grating into the uniform coupling region. We derive relations for the grating penetration slope—defined as $\alpha = L_p/L_g$, where L_p is the penetration depth at the design Bragg wavelength and L_g the grating length—which eventually determine the maximum allowed grating reflectivity. It should be stressed that the grating should be restricted inside the uniform waist-coupling region (of length L_w). Writing the grating in the tapered region of the coupler can severely deteriorate OADMs performance.

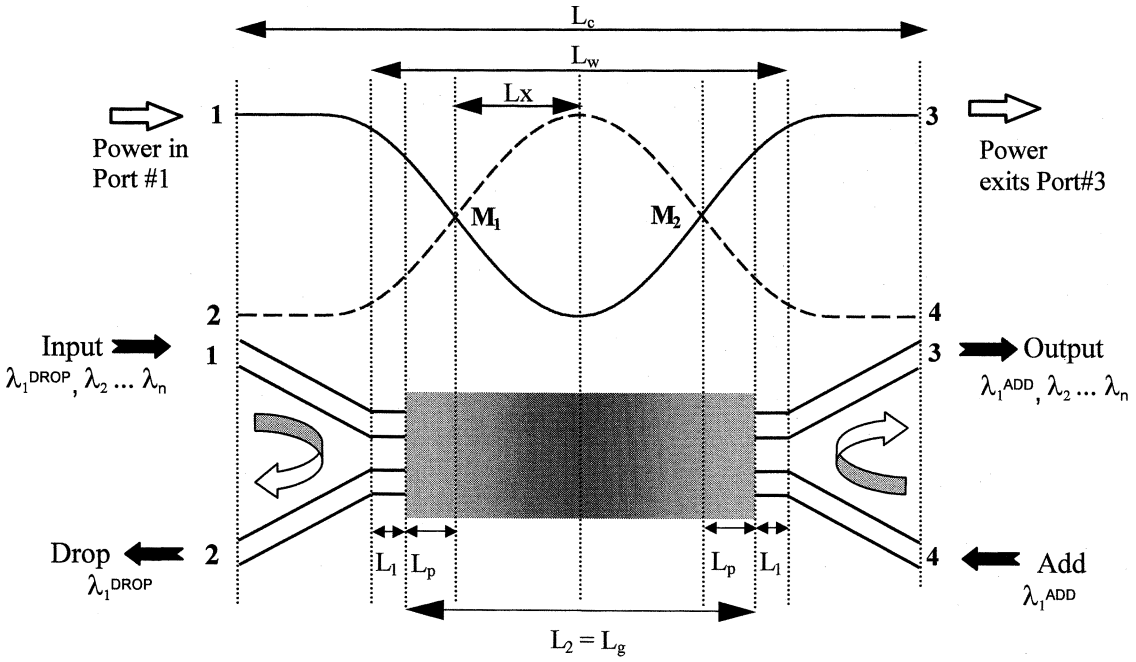

Fig. 3. Schematic of the FCC OADM with the power evolution along the full coupler. The configuration of the device is symmetric for optimized add–drop actions.

A. HCC-Based OADM

For systematic purposes we begin the study with the simplified case of the HCC configuration. We consider here a simplified case of grating arrangement, where at least, half of the coupler waist is used for the grating inscription $(L_3 = 0)$. We can write about the "geometrical" relation between the grating and the coupler (see Fig. 1) as

$$L_g = aL_g + \frac{L_w}{2}. \tag{4}$$

As it has already been mentioned, $L_g \leq L_w$, which leads to

$$L_g = \frac{L_w}{2(1-a)} < L_w \Rightarrow a \leq 0.5. \tag{5}$$

B. FCC-Based OADM

A similar relation can be derived for this full-cycle configuration. To keep this relation in simple form we can make the assumption that the length (M_1M_2) is equal to the half of the waist length L_w. This is equivalent to $L_w \cong 4L_x$ where L_x is the length corresponding to $\pi/2$ phase difference between the normal modes at the coupler waist. This simplification neglects basically the effect of the contribution of the tapered waveguide region to the phase evolution at the uniform waist region. We can now write (see Fig. 3)

$$L_g \cong 2aL_g + \frac{L_w}{2}. \tag{6}$$

Since $L_g \leq L_w$, similarly, we obtain the relation for the penetration slope, namely

$$L_g \cong \frac{L_w}{2(1-2a)} \leq L_w \Rightarrow a \leq 0.25. \tag{7}$$

If we consider the length L_x, we can form also another *exact* relation now, which gives the grating length

$$L_g = 2aL_g + 2L_x \Rightarrow L_g = \frac{2L_x}{(1-2a)}. \tag{8}$$

C. Multiple HCC-Based OADM

We can also generalize the derivation for the case of multiple (m) HCC-based OADM (see Fig. 4). In this case, the grating length can be expressed as

$$L_g = 2L_p + (2m-2)L_x \tag{9}$$

and taking into account that $L_p = \alpha \cdot L_g$ leads to the *exact* relation

$$L_g = \frac{2m-2}{1-2a}L_x \tag{10}$$

which will be referred to as the "*grating length equation*" from now on, because it relates the grating length to its own characteristics (through α) as well as the coupler characteristics (through L_x and m).

As already mentioned in the previous case of the *full cycle*, there is a finite contribution of the tapered waveguide region to the phase and consequently to the power evolution at the uniform waist region (Fig. 3). If we consider this contribution negligible (as illustrated in Fig. 4), we can write for the geometrical characteristics of the multiple HCC

$$L_x = \frac{L_w}{2m}. \tag{11}$$

Substituting (11) into (9), we derive

$$L_g = 2aL_g + \frac{2m-2}{2m}L_w \Rightarrow L_g = \frac{2m-2}{(1-2a)2m}L_w. \tag{12}$$

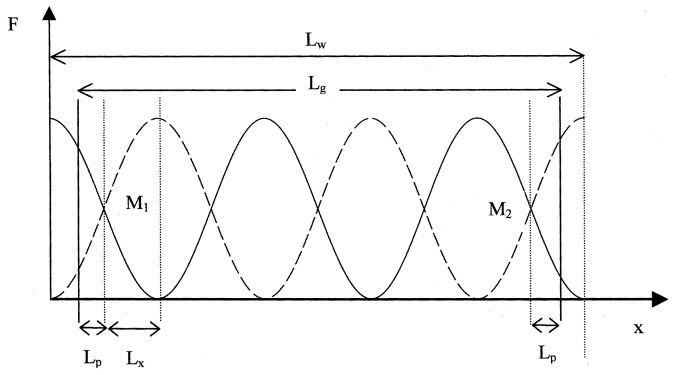

Fig. 4. Schematic of the optimum arrangement of a Bragg grating in a multiple HCC (here $m = 5$).

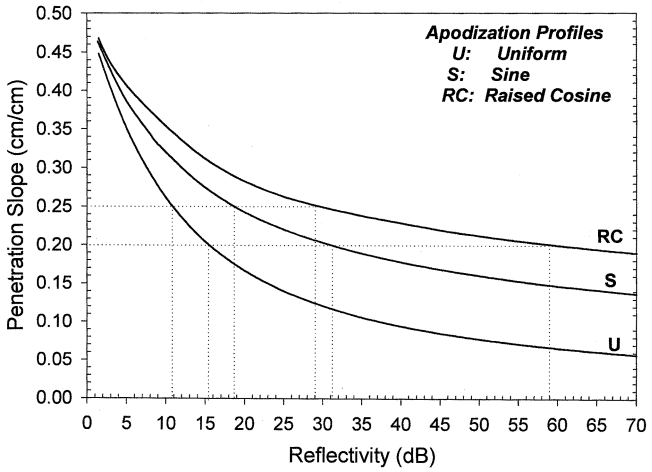

Fig. 5. Engineering curves for penetration slope versus reflectivity for various apodization profiles.

Again, imposing the limitation $L_g \leq L_w$ onto (12) results in

$$\frac{2m-2}{2(1-2a)m}L_w \leq L_w \Rightarrow \frac{2m-2}{2(1-2a)m} \leq 1 \Rightarrow a \leq \frac{1}{2m}. \tag{13}$$

Substituting $m = 1, 2$, we recover the previous results for the HCCs and FCCs given by (5) and (7), respectively.

We propose also and introduce generic engineering curves for Bragg gratings, which relate their penetration slope to their reflectivities for specific apodization profiles. We have found general engineering curves between the penetration slope and reflectivity for three different representative cases—a uniform, a sine apodised, and a raised cosine apodized grating. These general engineering curves are presented in Fig. 5. The significance of the "*grating length equation*" is greatly enhanced by the fact that the penetration slope of a grating for a specified apodization profile is related (by a "1–1" relation) to its reflectivity. The combination of the "*grating length equation*" with the grating engineering curves provides a powerful tool that can assist effectively in the design process of those OADM configurations.

One can notice at this point that the requirement for penetration slope is very tight for the multiple HCC-based OADM $(m > 1)$, whereas for the HCC. $(m = 1)$, there is not any restricting relation since $\alpha < 0.5$ always (α tends to 0.5 for very weak gratings and is decreasing for higher reflectivity). In contrast to the half cycle, in the full-cycle case, the grating should exhibit penetration slope less than an upper limit. For the theoretical obtained limit of 0.25, the grating would "cover" all the coupler waist length. Because of the effect of the taper region of the coupler, the actual maximum allowed slope is lower and thus for a reasonable coupler-waist coverage from the grating, we can set a value of about $\alpha \sim 0.2$.

For $\alpha = 0.2$, Fig. 5 gives minimum required reflectivities for different apodization profiles. These (absolute values) are at 15, 31, and 60 dB for uniform, sine, and raised cosine profiles, respectively. Thus, deployment of more drastic apodization profiles in order to suppress the dispersion effects of the grating, requires stronger gratings which in turn increase those effects, forming this way a restrictive tradeoff between the two parameters.

The value of α can be established much more accurately if the shape of the coupling region and the power evolution along the coupler is known. This can be measured accurately using nondestructive coupler characterization techniques [16].

D. Design Algorithm

The results of this discussion could be incorporated in the brief form of a design algorithm, which allows the determination of the length of a Bragg grating, with specified apodization profile and strength, in order to be located optimally inside a coupler's uniform waist.

We consider the general case of the multiple (m) HCC, and we assume that the effective refractive indexes of the even and odd normal modes are n_e, n_o, respectively. From the definition of the characteristic length L_x, we have the relation

$$(n_e - n_o)\frac{2\pi}{\lambda_o}L_x = \frac{\pi}{2} \tag{14}$$

which leads to

$$L_x = \frac{\lambda_o}{4(n_e - n_o)}. \tag{15}$$

For a specific grating apodization profile and reflectivity, the penetration slope (α) can be estimated by the engineering curves of Fig. 5. Beginning from the coupler characteristics (L_x, m) and the estimated penetration slope, the optimum grating length is calculated by the grating length equation (10). Finally, the maximum refractive index modulation is calculated for the required grating reflectivity. The design procedure is described schematically by the flow chart in Fig. 6.

V. Spectral Response of the FCC-Based OADM

Initially, we design an FCC in order to accommodate the Bragg grating which was deployed in Section II for the construction of the HCC OADM. By employing the same Bragg grating in a properly designed FCC, a symmetric and fully optimized OADM will now be exhibited. Starting from the length and the penetration depth of the grating, the required L_x parameter of the hosting coupler is calculated by (10) to be $L_x = 1.485$ mm. Based on that, we design a coupler with uniform waist of length

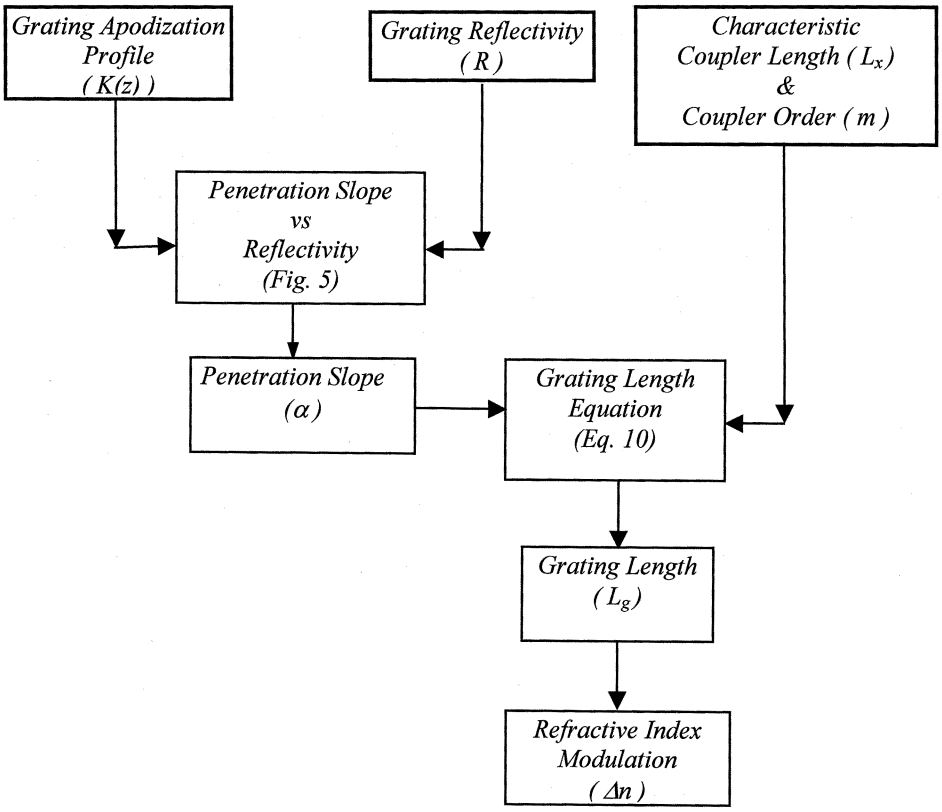

Fig. 6. Grating design algorithm for optimum inscription in a multiple HCC.

4.54 mm, which can accommodate the Bragg grating length of 4.5 mm. Placing the grating in to the center of the new FCC waist, we form the OADM. Fig. 7 plots the full response of the device which shows the simultaneously identical add and drop actions (R_{action}). Both actions exhibit now identical flat-top amplitude spectral response. The curves R_e and R_o represent the reflection spectra of the even and odd supemodes, respectively. We can notice that again, like the HCC case, the dispersion effects lead to considerable back reflections (R_{BR}) at the input. The -3-dB bandwidth of the drop–add action is now 0.7 nm, which implies a lower bandwidth utilization factor—compared with the half cycle—given that the inscripted grating exhibits bandwidth of 1 nm.

A. Spectral Response of Nonoptimally Designed FCC OADM

As demonstrated by the design algorithm, for a given FCC structure, there is a "1–1" exact relation between the reflectivity of the deployed Bragg grating and its physical length. Consequently, nonoptimum design and positioning of the grating into the coupler waist will lead to degraded device performance.

Degraded performance of the FCC OADM response due to a nonoptimimised inscripted grating is demonstrated by two examples. We consider the OADM device, which corresponds to the calculated reflection spectra shown in Fig. 7. The deployed grating is sine apodised with absolute reflectivity of 45 dB, and according to the proposed design method the optimal physical length is 4.5 mm.

In the first example, we form the OADM device by deploying a grating with absolute reflectivity 45 dB and length 2.5 mm. The full spectral response is shown in Fig. 8 where the associated loss of ~ -3 dB at the drop–add action and the very strong back reflections at the input port are clearly identified.

In the second example, we consider a grating with the optimized length of 4.5 mm but with (absolute) reflectivity of only 25 dB. The full response of the device is shown in Fig. 9, where the degraded characteristics are again obvious in there. The drop or add actions now exhibit a response with a much higher "$-3/-20$ dB" bandwidth ratio, which implies very poor bandwidth utilization factor in this nonoptimized configuration.

Generally, fabrication of those interferometric-based OADMs would require very accurate control for the proper inscription of the grating into the uniform coupling region. The precise characterization of the coupler is of critical importance for the successful inscription of the grating and the implementation of the device. An effective nondestructive coupler characterization technique applied to fiber couplers has recently been proposed for this purpose [16].

VI. Performance Characteristics of the HCC and FCC OADMs

This section presents results on the system performance characteristics of the HCC and FCC OADMs, thereby also providing a direct comparison. We consider initially the HCC OADM already studied in Section II, which will be referred to hereafter as *HCC-1*. The studied FCC OADM in Section V uses the same Bragg grating as the HCC-1, and its spectral response is shown in Fig. 7. Fig. 10 shows the reflectivity spectra of

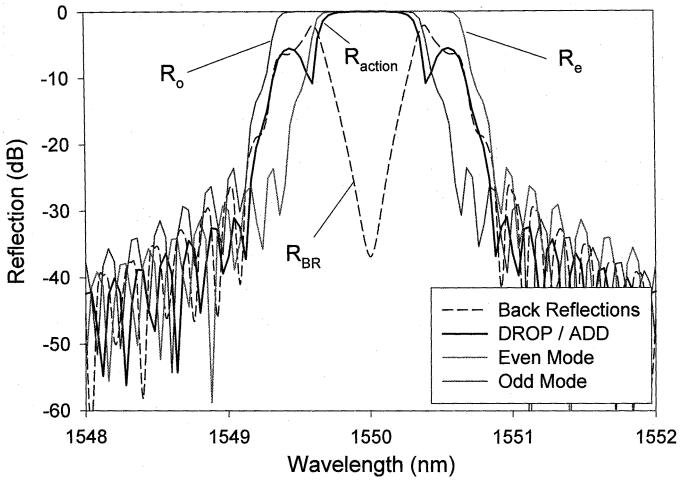

(a)

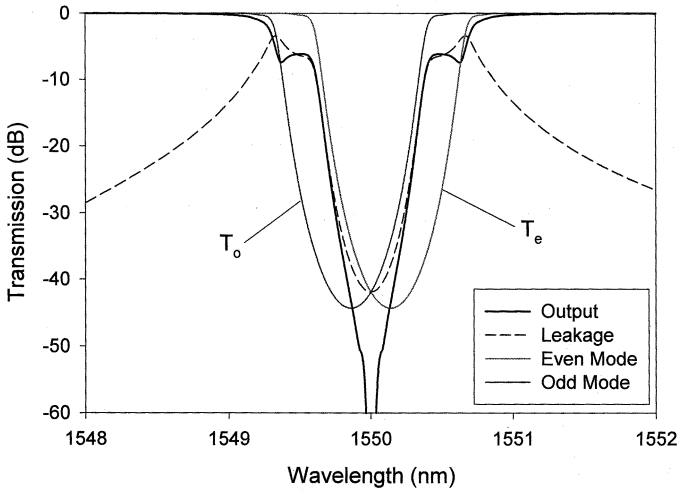

(b)

Fig. 7. Full spectral response of the FCC OADM. The drop–add actions are formed by the partial overlap of the even and odd modes reflection spectra. The optimally designed and deployed Bragg grating is sine apodized with length 4.5 mm and reflectivity of 45 dB.

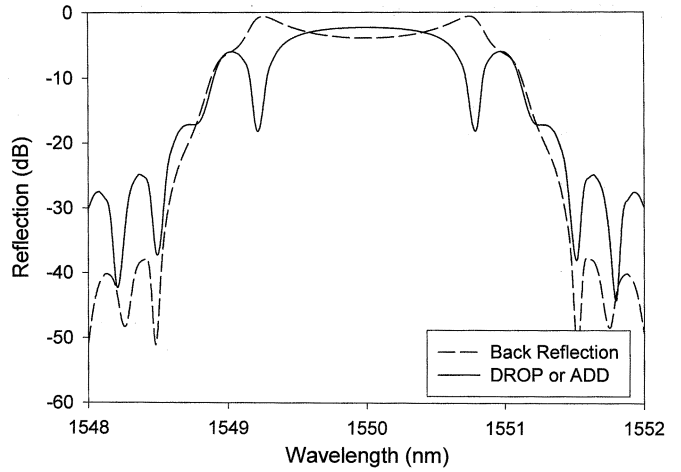

Fig. 8. Spectral response of a nonoptimally designed FCC OADM. The deployed grating exhibits the required reflectivity 45 dB, but the length is 2.5 mm.

these two OADMs, together with the reflectivity spectrum of the employed grating.

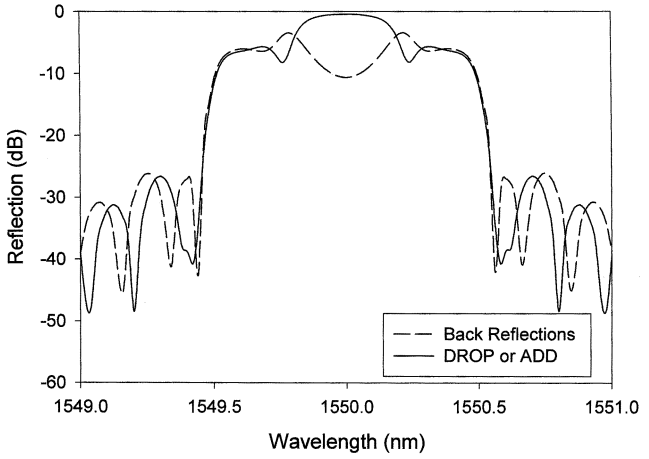

Fig. 9. Spectral response of a nonoptimally designed FCC OADM. The deployed grating is of optimum length 4.5 mm as in Fig. 6, but its reflectivity is only 25 dB.

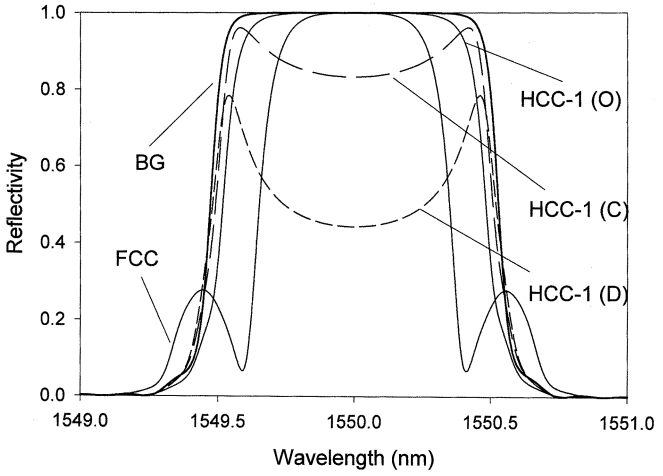

Fig. 10. Reflectivity spectra of the HCC-1 OADM for the optimized (O), compromised (C), and degraded (D) add–drop actions of a half-cycle-based OADM. Also shown is the reflectivity spectrum of the deployed grating (BG).

We consider also another HCC OADM referred to hereafter as *HCC-2 OADM*. This OADM is formed on the HCC we used for the *HCC-1 OADM* and is designed in order to exhibit a 3-dB bandwidth of $\sim$0.7 nm which is the same of the FCC OADM response. The Bragg grating now is of length $L_g = 5.2$ mm, amplitude of refractive index modulation $\Delta n = 3.65 \times 10^{-4}$, and uses a sine apodization profile. This bandwidth allows the study of its performance at 40-Gb/s (NRZ) transmission speed and a direct performance comparison to the *FCC OADM*. Fig. 11 shows and compares all these reflectivity spectra.

A. System Performance Simulation

The system performance of the interferometric OADMs is examined here by estimating the EOP in an IM/DD communication system. The simulated system is based on the synchronous optical network (SONET) standards, and the employed electrical filters at the transmitter and receiver are fourth-order Bessel filters with a 3-dB bandwidth 75% of the bit rate. A chirpless input is assumed into the OADMs by employing a balanced MZM. The input signal is a pseudorandom bit sequence (PRBS) of 2^7 b where by using fast Fourier transform (FFT) and inverse fast Fourier transform (IFFT), the

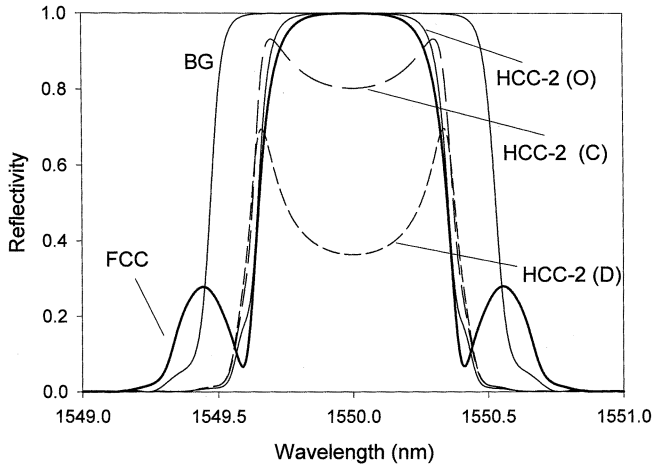

Fig. 11. Reflectivity spectra of the HCC-2 OADM for the optimized (O), compromised (C), and degraded (D) add–drop actions. Also shown, for comparison, is the reflectivity spectrum of the FCC OADM. The optimized response (O) of the HCC-2 OADM and the FCC OADM exhibits the same 3-dB bandwidth of 0.7 nm.

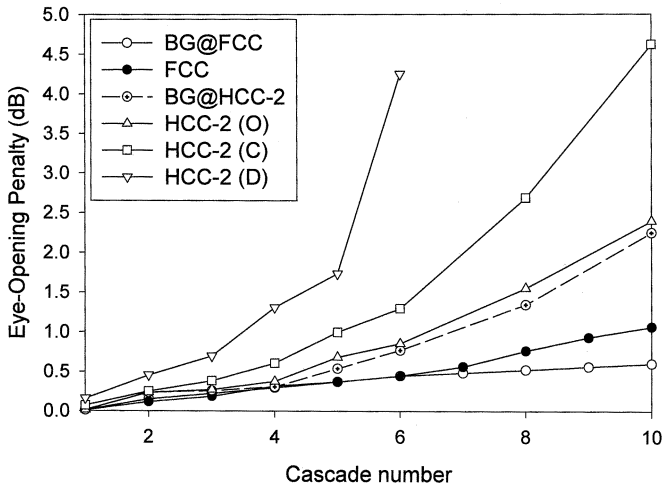

Fig. 12. Comparison of EOP performance between the HCC-2 OADM and the FCC OADM for cascaded filtering. EOP is estimated at 40 Gb/s as a function of the number of the perfectly aligned cascaded filters.

signal is converted from the time domain to frequency domain, and reverse. A more detailed description of the simulation method is contained in [14].

In the real case of a photonic network, a sequence of optical add–drop nodes can result in a number of *cascaded drop-and-add* operations. The performance of the filters is characterized here in such a cascaded operation. The filters are considered perfectly aligned with each other and aligned also with the center of wavelength-modulated signal spectrum.

B. Performance Comparison of HCC-2 OADM and FCC OADM

The HCC-2 OADM and the FCC OADM which exhibit the same −3-dB bandwidth of ∼0.7 nm are compared on their performance to cascaded operations. Fig. 12 gives the EOP of the FCC and HCC-2 filters as a function of the number of cascaded filters. Together are also shown two curves for the performance of the two employed Bragg gratings (BG@FCC and BG@HCC-2) with 1 and 0.79 nm 3-dB bandwidth, respectively. First, it is obvious that deployment of spectrally degraded filters

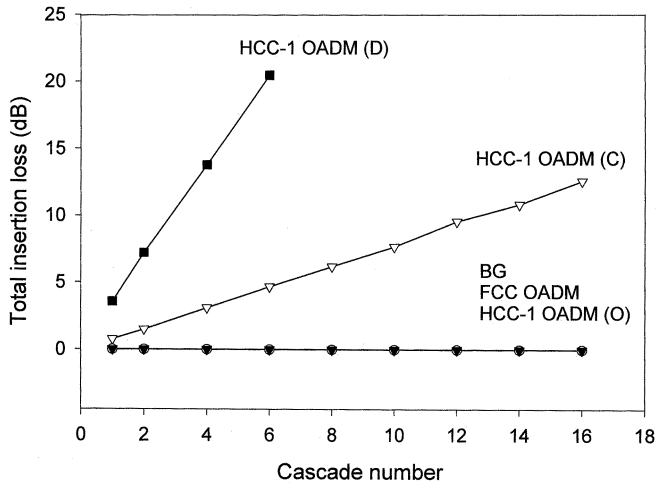

Fig. 13. Comparison of insertion loss for HCC and FCC OADMs in a cascaded filtering operation.

(C, D) results in higher EOP compared with the optimized case of the HCC-2 OADM. In this graph, we can note that despite their identical bandwidth, the FCC OADM exhibits lower EOP than the HCC-2 OADM. This can be explained by the in-band dispersion characteristics of the filters. Indeed, within the region of the 3-dB bandwidth, the FCC exhibits more flat dispersion characteristics compared with the HCC-2. This difference is due to the different characteristics of the employed gratings. The longer Bragg grating in the case of the HCC-2 OADM, which is required for the specified device's bandwidth (BW), is associated with stronger in-band dispersion [17] compared with the grating in the FCC OADM.

C. Performance Comparison of HCC-1 OADM and FCC OADM

From Figs. 10 and 11, the association of the nonoptimized spectral response of the HCC OADM with an additional insertion loss into the system is obvious. Fig. 13 gives a direct comparison of system excess loss for the HCC and FCC OADMs. Filters with spectrally flat-top response exhibit negligible insertion loss. From Fig. 10, the lower bandwidth utilization of the employed grating in the FCC OADM is clear. By using again system simulations, we quantify at 40 Gb/s the implications of OADMs bandwidth narrowing.

As in Fig. 12, the effect of cascading is studied again here and the resulting EOP performances are compared for the HCC-1 and FCC OADMs (Fig. 14). The EOP relation for the optimized (O) HCC OADM follows closely that of the BG. For a number of cascades less than eight, the FCC OADM performs as the other filters of much broader bandwidth. The compromised performance HCC (C) lies between that of FCC and BG. However, it should be emphasized here the apparent associated loss to this filter response (Fig. 13), which tends to the value of −15 dB for 16 cascades in contrast with the almost zero excess loss for the case of the FCC OADM.

VII. Summary

A novel interferometric OADM based on an FCC loaded with a Bragg grating has been proposed and theoretically analyzed. This OADM exhibits fully optimized and identical

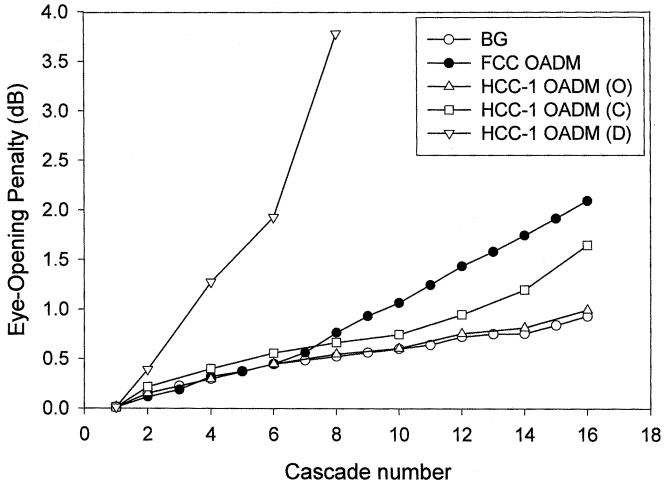

Fig. 14. Comparison of EOP performance between the FCC OADM and the HCC-1 OADM as a function of the number of cascaded filters. EOP is estimated for 40-Gb/s operation, and the cascaded filters are considered perfectly aligned to each other and to the center frequency of the signal spectrum.

add and drop actions due to its symmetric configuration and consequently symmetric operation [18]. The exhibited top-hat add–drop responses overcome the performance degradation due to distortion effects apparent in the HCC OADM where the add–drop actions are not simultaneously optimized.

More important, the new FCC OADM exhibits *uniform and negligible* insertion loss in contrast with the HCC OADM where the insertion loss depends on the particular configuration of the device and the particular orientation in the network of its employed ports. Thus, when in a WDM network a number of HCC OADMs are deployed, the insertion loss cannot be easily predicted because the loss contribution of each HCC OADM can be different. Consequently loss cannot be easily compensated.

For the effective design of the new FCC OADM, a general algorithmic method has been also proposed. The method is based on simple geometric relations between the grating and the coupler structure. Central to the design method is the existence of generic engineering curves—introduced here—which relates parameters such as the grating's penetration depth, reflectivity, and apodization profile.

Finally, the performance of the FCC OADM has been theoretically characterized using system simulations at transmission speeds of 40 Gb/s and compared directly to the HCC OADM performance.

REFERENCES

[1] K. P. Jones, M. S. Chadry, D. Simeonidou, N. H. Taylor, and P. R. Morkel, "Optical wavelength add-drop multiplexer in installed submarine WDM network," *Electron. Lett.*, vol. 31, no. 24, pp. 2117–2118, Nov. 1995.

[2] L. Dong, P. Hua, T. A. Birks, L. Reekie, and P. St. Russell, "Novel add–drop filters for wavelength-division multiplexing optical fiber systems using a Bragg grating assisted mismatched coupler," *IEEE Photon. Technol. Lett.*, vol. 8, pp. 1656–1658, Dec. 1996.

[3] A. S. Kewitsch, G. A. Rakuljic, P. A. Willems, and A. Yariv, "All fiber zero insertion loss add drop filter for WDM," *Opt. Lett.*, vol. 23, no. 2, pp. 106–108, Jan. 1998.

[4] C. Riziotis and M. N. Zervas, "Design considerations of optical add–drop filters based on grating assisted mode conversion in null couplers," *J. Lightwave Technol.*, vol. 19, pp. 92–104, Jan. 2001.

[5] T. Erdogan, "Optical add–drop multiplexer based on asymmetric Bragg coupler," *Opt. Commun.*, vol. 157, pp. 249–264, Dec. 1998.

[6] D. C. Johnson, K. O. Hill, F. Bilodeau, and S. Faucher, "New design concept for a narrowband wavelength-selective optical tap and combiner," *Electron. Lett.*, vol. 23, pp. 668–669, 1987.

[7] F. Bilodeau, D. C. Johnson, S. Theriault, B. Malo, J. Albert, and K. O. Hill, "An all-fiber dense-wavelength-division multiplexer/demultiplexer using photoimprinted Bragg gratings," *IEEE Photon. Technol. Lett.*, vol. 7, pp. 388–390, Apr. 1995.

[8] J. Albert, F. Bilodeau, D. C. Johnson, K. O. Hill, K. Hattori, T. Kitagawa, Y. Hibino, and M. Abe, "Low-loss planar lightwave circuit OADM with high isolation and no polarization dependence," *IEEE Photon. Technol. Lett.*, vol. 11, pp. 346–348, Mar. 1999.

[9] T. Erdogan, T. A. Strasser, M. A. Milbrodt, E. J. Laskowski, C. H. Henry, and G. E. Kohnke, "Integrated-optical Mach–Zehnder add–drop filter fabricated by a single UV-induced grating exposure," *Appl. Opt.*, vol. 36, pp. 7838–7845, 1997.

[10] R. Kashyap, G. D. Maxwell, and B. J. Ainslie, "Laser-trimmed four-port bandpass filter fabricated in single-mode photosensitive Ge-doped planar waveguide," *IEEE Photon. Technol. Lett.*, vol. 5, pp. 191–194, Feb. 1993.

[11] K. Bakhti, P. Sansonetti, C. Sinet, L. Gasca, L. Martineau, S. Lacroix, X. Daxhelet, and F. Gonthier, "Optical add–drop multiplexer based on UV written Bragg gratings in a fused 100% coupler," *Electron. Lett.*, vol. 33, no. 9, pp. 803–804, Apr. 1997.

[12] F. Bakhti, X. Daxhelet, P. Sansonetti, and S. Lacroix, "Influence of Bragg grating location in fused 100% coupler for add and drop multiplexer realization," in *OFC 98 Tech. Dig.*, 1998, Paper ThQ2, pp. 333–334.

[13] C. Riziotis, P. G. R. Smith, and M. N. Zervas, "Performance characteristics of interferometric Bragg grating based OADM's in WDM transmission systems," in *Tech. Dig. OSA Int. Conf. Bragg Gratings, Photosensitivity Poling Glass Waveguide, BGPP 2001*, Stresa, Italy, July 4–6, 2001, Paper BThC2.

[14] C. Riziotis and M. N. Zervas, "Performance comparison of Bragg grating-based optical add–drop multiplexers in WDM transmission systems," *Instit. Elect. Eng. Proc. Circuits Devices Systems*, vol. 149, no. 3, pp. 179–186, June 2002.

[15] E. Marin, R. Ghosh, J.-P. Meunier, X. Daxhelet, and S. Lacroix, "Bragg gratings in 2 × 2 symmetric fused fiber couplers: Influence of the tilt on the wavelength response," *IEEE Photon. Technol. Lett.*, vol. 11, pp. 1434–1436, Nov. 1999.

[16] C. Alegria, F. Ghiringhelli, and M. N. Zervas, "Non-destructive characterization of fiber couplers," in *Proc. ECOC '01*, Amsterdam, The Netherlands, Sept. 30–Oct. 4 2001, Paper We.L.2.3.

[17] M. Ibsen, H. Geiger, and R. I. Laming, "In-band dispersion limitations of uniform apodised fiber gratings," in *Proc. ECOC '98*, Madrid, Spain, Sept. 20–24, 1998, Paper WdA16.

[18] C. Riziotis and M. N. Zervas, "WaveGuide Coupler Optical Add/Drop Multiplexer," EU/US Patent No. 02253113.1, May 2002.

Christos Riziotis (M'01) was born on December 24, 1970 in Farsala, Greece. He received the physics degree and the M.Sc. degree in electronics and telecommunications from the National and Capodistrian University of Athens, Athens, Greece, in 1993 and 1995, respectively, and the Ph.D. degree in optoelectronics and optical communications from the Optoelectronics Research Center (ORC), University of Southampton, Southampton, U.K., in 2001.

From 1996 to 1997, he did his military service in Hellenic Army Aviation as an Aircraft Engineer. In 1997, he joined ORC and worked in the areas of photonic materials, Bragg-grating-based devices, design and fabrication of integrated dense-wavelength-division-multiplexing (DWDM) devices, and optical communication systems. In 2000, he was appointed Research Fellow at ORC, where he was responsible for the world-class Direct UV-Writing Facility for the fabrication of integrated planar devices. Since 2002, he had been working in TEMAGON, the technology consulting branch of the Hellenic Telecommunications Organization (OTE Group), where he was involved in the technical and regulatory issues of telecommunications and IT. Since 2002 to present, he has been working as a Research Associate at Optical Communications Laboratory, University of Athens, focusing in the area of high-speed communication systems. To date, he has produced more than 25 technical publications in various areas of photonics and optical communications and has two patents/patent applications.

Dr. Riziotis is a Member of the Optical Society of America (OSA) and he is serving as a Technical Reviewer for IEEE and OSA publications.

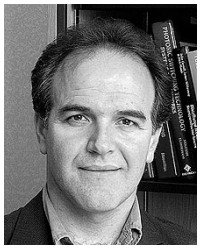

Mikhail N. Zervas (S'88–M'88) was born on June 1, 1959 in Dimaina, Nafplion, Greece. He graduated from the Electrical Engineering Department, University of Thessaloniki, Greece, in 1984 and received the M.Sc. degree in applied and modern optics from the University of Reading in 1985 and the Ph.D. degree in fiber optics from the University College London, London, U.K., in 1989.

He joined the Optoelectronics Research Centre, University of Southampton, Southampton, U.K., in 1991 as a Research Fellow and was promoted to Research Lecturer in 1995 and Professor in Optical Communications in 1999. His research activities include surface-plasmon effects and devices, optical trapping and nano-particle manilulation, advanced optical fiber amplifier configurations, high-power fiber lasers, fiber distributed feedback lasers, and Bragg grating theory and devices. He is one of the cofounders of Southampton Photonics Inc., and he is currently on a university sabbatical leave serving as Chief Scientist at SPI. He has authored/coauthored more than 160 technical publications and 20 patents/patent applications and has served on various conference program committees. He was the general program co-chair of the 1999 Optical Amplifiers Meeting [Optical Society of America (OSA)] in Japan. He has given a number of invited talks and short courses in fiber gratings and fiber amplifiers at major international conferences. He was a coeditor of a Special Issue on Fiber Bragg Gratings for the journal *Integrated and Fiber Optics*.

Dr. Zervas shared with his colleagues the prestigious Metrology award from the Confederation of British Industry in 1996 for their work on grating measuring systems for characterizing reflection and dispersion performance of fiber Bragg gratings.